Carland, E. M., P. R. Stoddart, P. J. Cadusch, J. B. Fallon, and S. A. Wade. 2016. Effect of embedded optical fibres on the mechanical properties of cochlear electrode arrays, Medical Engineering & Physics, 38: 155-62.

Effect of embedded optical fibres on the mechanical properties of cochlear electrode arrays

Emma M Carland[a], Paul R Stoddart[a], Peter J Cadusch[b], James B Fallon[c,d], Scott A Wade[b,*]

[a]*ARC Training Centre in Biodevices, Swinburne University of Technology, Hawthorn, Victoria, Australia*

[b]*Faculty of Science Engineering and Technology, Swinburne University of Technology, Hawthorn, Victoria, Australia*

[c]*The Bionics Institute, East Melbourne, Victoria, Australia*

[d]*Medical Bionics Department, University of Melbourne, Parkville, Victoria, Australia*

Keywords: Cochlear implant, Optical fibre, Stiffness, Electrode array

*Corresponding Author. Tel. +61 3 9214 4339

E-mail address: swade@swin.edu.au (S.A. Wade)

Abstract

Incorporating optical fibres in cochlear electrode arrays has been proposed to provide sensors to help minimise insertion trauma and also for the delivery of light in optical nerve stimulation applications. However, embedding an optical fibre into an electrode array may change its stiffness properties, which can affect the level of trauma during insertion. This report uses measurements of buckling and deflection force to compare the stiffness properties of a range of cochlear electrode arrays (Nucleus straight array, rat array, cat array and guinea pig array) with custom arrays containing an embedded optical fibre. The cladding diameters of the optical fibres tested were 125 µm, 80 µm and 50 µm. The results show that the stiffness of the optical-fibre-embedded arrays is related to the diameter of the optical fibre. Comparison with wired arrays suggests optical fibres with a diameter of 50 µm could be embedded into an electrode array without significantly changing the stiffness properties of the array.

1. Introduction

Over the past 30 years, cochlear implants have helped many recipients who have severe to profound deafness to hear [1, 2]. The cochlear implant system consists of a microphone, speech processor, transmission system, stimulator and an electrode array that is implanted into the cochlea [1]. The electrode array plays a crucial role in activating the auditory neurons [3].

The cochlea is an extremely delicate structure. Therefore, while cochlear implants have proven to be an effective intervention, there has been an ongoing effort to identify ways of minimising any potential trauma to the cochlea due to the electrode array insertion process [4-9]. The interested reader is directed to references [1] and [9] for a more detailed description of the cochlear anatomy. Damage to the basilar membrane and to the spiral ligament at the outer wall of the scala tympani are some negative outcomes potentially associated with the insertion of cochlear implant electrode arrays [3, 9, 10]. Injury to the functional peripheral dendrites or spiral ganglion cells during insertion can lead to reduced efficiency of the cochlear implant system [11]. Insertion trauma can also effect the positioning of the cochlear electrode [12] which may impair performance. Recently there has been a growing trend of cochlear electrode implantation in partially deaf patients [13]. These patients commonly have good low frequency hearing [14]. The importance of atraumatic implant insertion is increased

due to the desire to preserve this hearing as it has been shown to improve speech recognition in noisy environments and the appreciation of music [13-18].

Improved implant designs and insertion techniques have significantly reduced the potential for insertion trauma [19]. In order to further reduce the instances and/or extent of insertion trauma there has been interest in including sensors in the electrode array to provide real-time feedback to the surgeon, or as part of a robotic insertion tool [20, 21]. Feedback could include information on the force, position and/or curvature of the electrode array during the insertion process [9, 22-27]. Optical fibre sensors embedded into the electrode array may be able to provide this feedback and therefore help to reduce insertion trauma [9].

Optical fibres are thin light guiding structures typically made from silica glass. The most well-known use of optical fibres is in telecommunication applications, however they are also widely utilised in sensing devices [28]. Common single mode optical fibre has three layers: the innermost light guiding layer is the glass core, which is surrounded by a glass cladding and an outer protective acrylate coating, as shown in the insert of Fig. 1.

In general optical fibre sensors have advantages of being safe, flexible, small, and reliable [28]. Optical fibre sensors can be used to sense a variety of parameters including strain/force, temperature and bending [28]. For example, an optical fibre Bragg grating sensor embedded in a cochlear electrode array has been used to monitor the force acting on the tip of the array [9]. Optical fibre has also been suggested as an acoustic sensor within the cochlear implant allowing for a completely implantable system [27] and has been proposed to deliver light for optical stimulation of the cochlea [29-31]. Recently Balster and co-workers investigated the insertion forces of optical fibres in a cochlear model and also human temporal bones in relation to optical stimulation [32]. They found that the insertion forces in the model and trauma in temporal bones both reduced with smaller fibre diameters.

The stiffness of cochlear electrode arrays have been shown to be related to the amount of subsequent insertion trauma [3, 4, 6, 7, 11, 33]. The stiffness of an electrode array affects its ability to withstand deformation [34] and takes into account the Young's modulus, shape and boundary conditions of the material(s) with which the array is made. For example, finite element modelling has suggested that the Nucleus straight array design may be less likely to create insertion trauma compared to the Nucleus contour array design (both by Cochlear Ltd) [3]. The Nucleus straight array has a graded stiffness [33], which reduces the contact pressure exerted by the tip of the electrode array [4].

Embedding an optical fibre into an electrode array may change its stiffness properties. Therefore this work aims to compare the stiffness properties of optical-fibre-embedded electrode arrays with conventional cochlear electrode arrays and also with a number of custom arrays used in animal trials. In the embedded optical fibre arrays, the electrode wires were replaced with optical fibres with diameters in the range of 50 – 125 μm. This study aims to clarify what changes to mechanical properties result from incorporating an optical fibre into an electrode array.

2. Theory

The stiffness properties of cochlear electrode arrays can be investigated by looking at the deflection and buckling forces. These forces represent the transverse and longitudinal forces acting on the electrode arrays during insertion.

2.1 Deflection Force

The deflection force, P is the force required to deflect an object a certain distance, δ_{max}, as shown in Fig. 1. This force is directly related to the stiffness of an object, as it is this force that overcomes the object's resistance to deflection. Measurements of deflection force have previously been used to determine the stiffness of cochlear electrode arrays [7, 11, 33]. For example, Kha *et al* [33] showed that the stiffness of the Nucleus straight array (Cochlear Ltd) varies along the length of the array.

The deflection force of the electrodes can be modelled according to the cantilever beam theory [35] for a concentrated load, *P*, applied on the beam at any point. The experimental arrangement used for deflection force testing in this work is shown in Fig. 1. The deflection distance, δ_{max}, for a given force, *P*, applied at a location l along a beam of total length *L*, can be calculated using [35]:

$$\delta_{max} = \frac{Pl^2}{6EI}(2l + 3b), \quad (1)$$

where *E* is Young's modulus (72.5 GPa for silica fibre [36]) and the moment of inertia, *I*, is given by

$$I = \frac{\pi d^4}{64} \quad (2)$$

for a beam of diameter *d*. See Fig. 1 for further explanation of the relevant parameters.

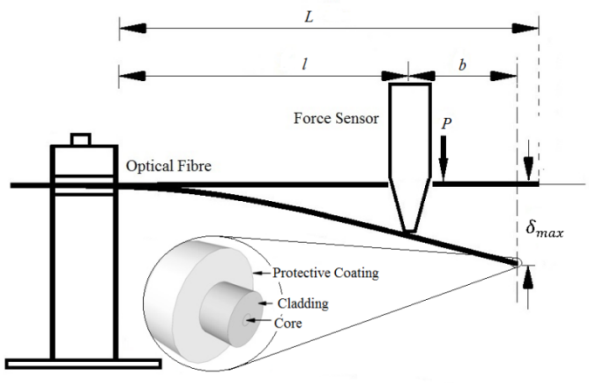

Fig. 1. Cantilever beam test configuration showing the parameters used in testing and calculating the theoretical stiffness of the beam. Insert shows the optical fibre structure (not to scale).

This theory is based on a small bending approximation which in reality is not completely appropriate for this work. In particular, assumed uniform beam stiffness and diameter, excludes the effects of friction (between array/fibre and force sensor) and assumes that the bending angle is very small, whereas the angle used is relatively large (up to 30 degrees). As such a more general theory was derived to better match the actual test case. This theory is referred to as the derived theory in this paper. For more information on the derived theory, please refer to the supplementary material, S1.

2.2 Buckling Force

The buckling force is the force required to buckle/bend a beam (e.g. the electrode array) when it is subjected to a compressive force in the longitudinal direction (see Fig. 2). Patrick and MacFarlane [7] found that the buckling force of the Nucleus array was 0.5 g (equivalent to 4.9 mN). They also found that this low buckling force for a tapered electrode array reduced the likelihood of injury to the cochlea during insertion compared to a solid wire electrode (buckling force 12.5 g or 122.5 mN). The buckling force can be modelled using the bifurcation buckling force theory [37], where the buckling force (F_B) is given by:

$$F_B = \frac{EI\pi^2}{{l_e}^2}, \quad (3)$$

where *E* is the Young's modulus as in equation (1), *I* was defined in equation (2) and

$$l_e = kL \quad (4)$$

is the effective length, which depends on the way that the object is held. The condition that best represents a cochlear electrode array as it is inserted into the cochlea is the fixed-pinned condition, i.e. rotation- and

translation-fixed at one end, but rotation-free and translation-fixed at the other, as shown in Fig. 2. For this situation k= 0.7.

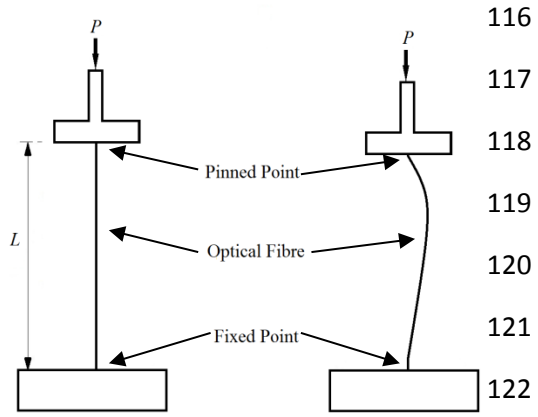

Fig. 2. The fixed-pinned test configuration in which the optical fibre was held for buckling tests.

3. Experimental Method

Stiffness testing of electrode arrays and optical fibres was completed in two sections: deflection force testing and buckling force testing. All testing was performed using three different diameters of optical fibre, namely 50 µm diameter (Fibercore, SM1500), 80 µm diameter (Newport Corporation, F-SBD) and 125 µm diameter (Corning, SMF-28). For most of the testing procedure the protective acrylate coating was left on the optical fibres, except at the tip where it was removed using a mechanical stripping tool for the 125 and 80 µm diameter fibre and paint stripper for the 50 µm diameter fibre. This section of the coating was removed in order to allow the tip of the optical fibre to be cleaved at 90° (unless otherwise specified). After cleaving a length of approximately 6 mm at the end of the fibre was left without the acrylate coating.

3.1 Deflection Force

The deflection force was measured for five different wired cochlear electrodes, including two Nucleus straight arrays, a rat array, a cat array and a guinea pig array. The results were compared with measurements obtained for plain optical fibres and for optical-fibre-embedded electrode arrays, which were specially manufactured for this work by replacing the metal wires with a single optical fibre. The outer diameter of the rat array is 0.4 mm at the tip and 0.8 mm at the base [38]. This array design has 3 platinum electrodes with platinum/iridium wires at the tip of the array and two reference electrodes (without wires) 4 mm and 6 mm from the tip. The guinea pig electrode array has three platinum electrodes connected to platinum/iridium wires at the tip of the array. A reference electrode is also positioned 5 mm from the tip of the electrode. The diameter of the guinea pig electrode array is 0.5 mm at the tip and 0.8 mm at the base [39, 40]. The cat electrode array has 8 platinum electrodes along the tip of the array spaced 0.3 mm apart with platinum/iridium wires attached. The diameter of the electrode array is 0.4 mm at the tip and 0.7 mm at the base [41, 42]. The Nucleus straight array (Cochlear Ltd) has 32 platinum electrodes of 0.3 mm width positioned along the length of the array. Of these electrodes 22 are connected to Teflon coated electrode wires. The diameter of the electrode array is 0.45 mm at the tip and 0.7 mm at the base [4, 33, 43].

For the optical-fibre-embedded electrode arrays, samples of the optical fibres previously mentioned (50 µm, 80 µm and 125 µm cladding diameter) were embedded in Silastic (MED1-4213, NuSil). The optical-fibre-embedded electrode arrays were 0.6 mm at the tip and 0.9 mm at the base with three unwired platinum reference ring electrodes (0.2 mm wide, 0.4 mm diameter, 1.2 mm spacing between the first and second electrode and 1.9 mm spacing between the second and third electrode) included at the tip of the array. This is a similar configuration to the guinea pig arrays. The array was fabricated by injection moulding process, which helped to ensure that the optical fibre was located close to the centre of the cylindrical array. To determine the effect of

metal wires in the array, deflection tests were also performed on an 80 µm optical-fibre-embedded in Silastic with the three electrodes welded to platinum/iridium wires (25 µm diameter). Experiments were also completed on plain optical fibre (i.e. not embedded), and for one of the fibre types (125 µm diameter) with the acrylate coating removed from the complete length. Some of the electrode arrays used in this study are shown in Fig. 3.

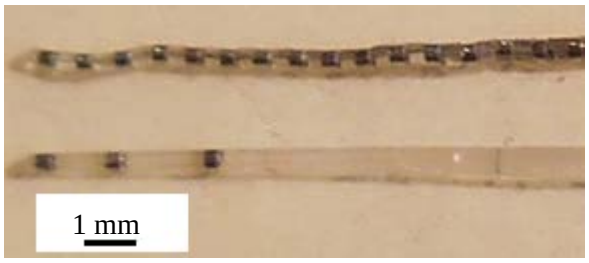

Fig. 3. Photos of electrode array examples. Top: Nucleus straight array. Bottom: 125 µm optical-fibre-embedded electrode array.

Deflection force tests were conducted based on the theory of a cantilever beam with a load concentrated at varying points along the beam (i.e. electrode array) [35]. The electrode array was secured horizontally at the base using a custom fixture as shown in Figs. 1 and 4. A vertical force was applied to the array at varying distances, l, from the fixed point using a force gauge (Mark-10, 5i) with a force resolution of 0.1 mN. For each load point the magnitude of load applied was such that there was a constant overall deflection distance, δ_{max} at the end of the beam/electrode. This corresponded to a deflection angle of 30° as $l \rightarrow 0$, which is the same angle of deflection used by Rebscher *et al*. in their study of the stiffness properties of wired electrode arrays [11]. The force required to deflect the electrode to this position at different values of l was recorded. The deflection force was recorded four times at each point l.

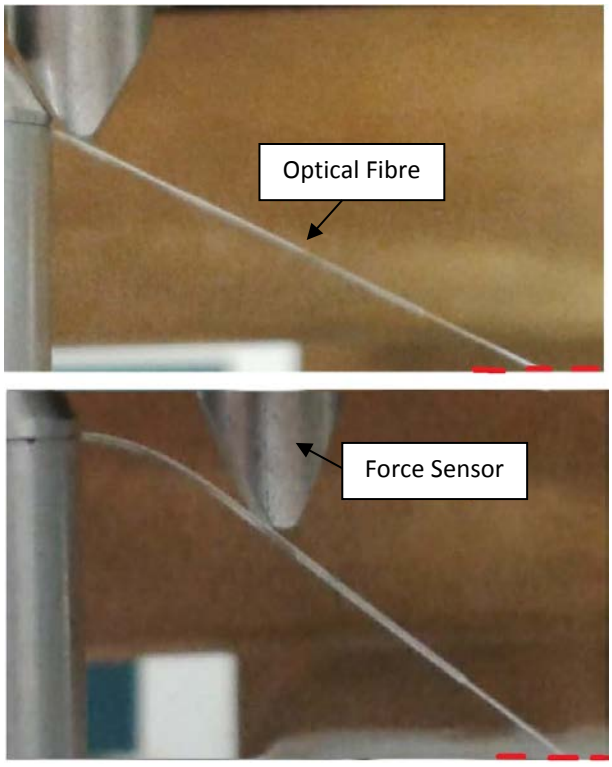

Fig. 4. Two examples of deflection tests on optical fibre. In these tests a wedge attachment on the force sensor was used to deflect the fibre/electrode array by applying a load at different points. The dashed red line represents the distance to which the optical fibre was deflected in each test example.

3.2 Buckling Force

Buckling force tests were performed using plain non-embedded optical fibres (50 µm, 80 µm and 125 µm cladding diameter). Although the results of the deflection tests, which were preformed first, showed that there was a difference between the embedded and non-embedded optical fibres (in magnitude only) especially at the lower diameters, it was decided that for simplicity the buckling force tests would only be completed on plain optical fibre. The optical-fibre-embedded electrode arrays were not used in the buckling tests because of difficulties in mounting them vertically: they tended to slide at the pinned point and bend due to their low stiffness and the weight of the Silastic. There was also an issue with the end of the array not being flat, as this can lead to variability in results. The buckling tests were based on the bifurcation buckling theory [37] and followed the same basic experimental procedure as Patrick and MacFarlane [7]. The test set up utilised the fixed-pinned configuration for bifurcation buckling as this is considered to be the condition that best represents electrode arrays during insertion into the cochlea.

In order to perform the buckling force tests, a length of acrylate coating on the optical fibres was stripped as described previously and the fibres were cleaved at 90º at the end to which the load was subsequently applied. The fibres were then secured vertically in an optical fibre chuck which provided the "fixed" point. A Labview-controlled Newport ILS 100 PP translation stage powered by a Newport EPS 300 driver was used to lower a force sensor (Mark-10 5i, 0.1 mN accuracy) with a flat plate attachment onto the "pinned" tip of the optical fibre until it buckled. To ensure reproducible results, the force plate of the force sensor was polished to a mirror finish (final polish with a colloidal silica suspension of 0.05 µm). During the buckling tests data from the force sensor was gathered at a sampling interval of 12 ms by a USB oscilloscope (Stingray, DS1M12).

The force sensor was moved onto the tip of the optical fibre at a rate of 0.2 mm/s. This speed was a compromise between completing the testing in a timely manner while ensuring adequate sampling resolution at the time when buckling occurs. Data were collected for different optical fibre lengths (length of optical fibre exposed from the top of the fibre chuck). An example of the raw data from which the buckling force was determined can be found in the supplementary material, S2.

Results

4.1 Deflection Force

The deflection testing results for optical-fibre-embedded electrode arrays are shown in Fig. 5, with each point representing the mean of at least four recordings. The error bars indicate the spread of the measured data (±(max-min)/2). For comparison purposes the cantilever beam theory (Eq. 1) was plotted on the same graph as the results (solid line) and a curve using the derived theory is also shown (dashed line). The results have a relatively poor correspondence with the cantilever beam theory, but show a somewhat improved fit with the derived theory. In general the shape of the curve of the experimental results is in agreement with the theory, but the magnitude of the results is shifted from the predicted value. For most of the results the derived theory appears to be closer to the recorded results. The only recorded exception is with the 50 µm results at higher load location points (above 10 mm approx.). The stiffness properties of the optical-fibre-embedded electrode arrays were primarily determined by the optical fibre diameter. The stiffness of the embedded electrode arrays decreased with reduction in the diameter of the embedded optical fibre, for all load locations.

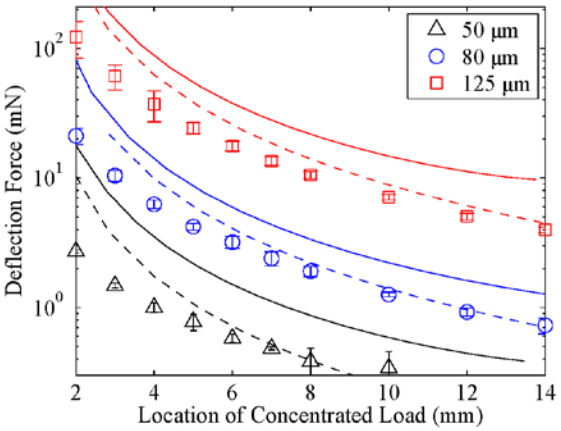

Fig. 5. The results of 30° deflection testing of the optical-fibre-embedded electrode arrays, together with theoretical curves (cantilever beam theory = solid line, derived theory = dashed line).

Measurements of deflection force for the animal and human cochlear electrode arrays are shown in Fig. 6 together with solid lines representing theoretical fits (cantilever beam theory, Eq 1). The results suggest that the electrode array embedded with a 125 µm diameter optical fibre would be stiffer than or comparable to any of the animal or human electrode arrays tested across the range of load location points tested. The stiffness of the Nucleus straight cochlear electrode (average of two Nucleus straight array electrodes tested) was found to be between the 125 µm and 80 µm embedded optical fibre electrode arrays. The 50 µm optical-fibre-embedded array was found to have the lowest stiffness overall of any of the electrode arrays tested. The guinea pig electrode array displayed similar stiffness properties to the 80 µm embedded optical fibre electrode array. The cat and rat electrode arrays had stiffness properties similar to the 50 µm embedded electrode array at small values of l, but had stiffness properties closer to the 80 µm embedded optical fibre electrode array at higher values of l.

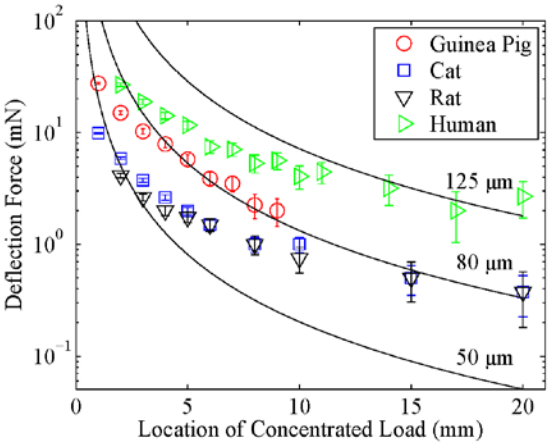

Fig. 6. Experimental results of 30° deflection force for a range of wired cochlear electrode arrays compared with theoretical curves (cantilever beam theory) for embedded optical fibres.

The measurements for the wired electrodes shown in Fig. 6 have a relatively poor fit to the cantilever beam theory (Eq. 1). It can be seen in Fig. 6 that the experimental curves for the electrode arrays are flatter than the general form of the theory curves. The standard cantilever beam theory (i.e. Eq. 1) assumes a constant stiffness along the beam length, which is not consistent for example with the stiffness profile of the Nucleus straight array (Cochlear Ltd) [33]. The data for the animal electrode arrays exhibit a similar trend to the Nucleus straight array, suggesting that their stiffness profile is also graded. This may be the reason for the relatively poor fit of the cantilever theory in this case.

The results in Fig. 7a show that similar deflection measurements were obtained for an optical-fibre-embedded electrode array (125 µm), stripped optical fibre (125 µm) and plain (acrylate coated) 125 µm diameter fibre. This result may be due to the fact that the increased stiffness and diameter of the 125 µm diameter optical fibre mean that the result is less affected by other factors such as the Silastic coating. It is interesting to note that the theory curves shown in Fig. 7a predict a small difference in the magnitude of the deflection force when changing the fibre conditions as mentioned. The theory predicts that the embedded fibre would be the stiffest followed by the plain fibre and then the stripped fibre. These differences however are not predicted to be large and may be hidden in the error of the measured values. Fig. 7a also shows that the theory is slightly higher in magnitude than the data for small values of l, but is closer to the recorded values at larger values.

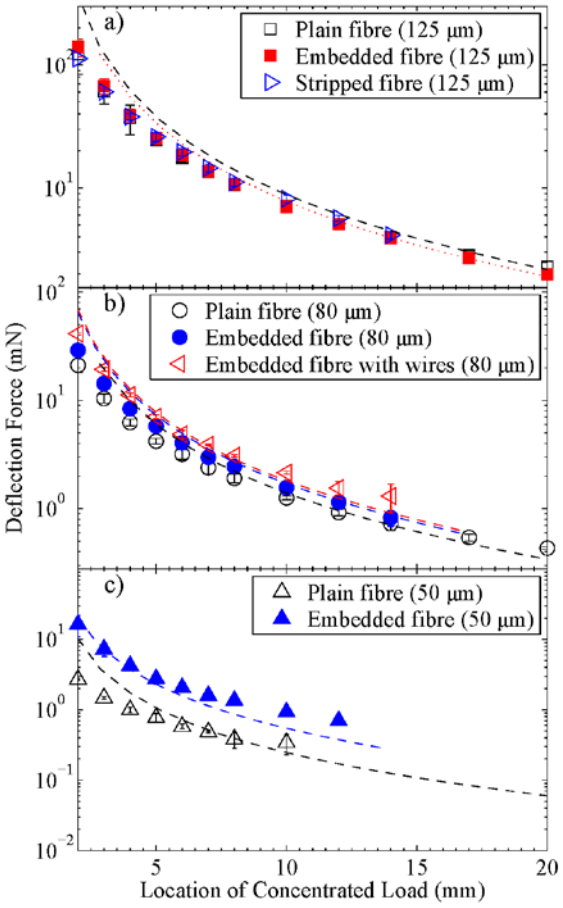

Fig. 7. Results of 30° deflection tests for: **a)** 125 µm optical-fibre-embedded electrode arrays, plain optical fibre and stripped optical fibre compared to the derived theory (dashed lines); **b)** 80 µm optical-fibre-embedded electrode arrays with and without wires and plain optical fibre compared to the derived theory (dashed line); and **c)** 50 µm optical-fibre-embedded electrode arrays and plain optical fibre compared to the derived theory (dashed line). Note that data was not taken at longer lengths for the 50 µm fibre as the forces were too low to measure with the force sensor used in the experiment.

For the 80 µm optical fibre, the plain fibre was found to be slightly less stiff than the fibre embedded in the array, which in turn was slightly less stiff than the fibre embedded in the array with wires. These results are plotted together with the derived theory (dashed lines) in Fig 7b. The differences are small but consistent. This suggests that in this case the stiffness properties of the electrodes arrays are still largely dominated by the 80 µm optical fibre. The measurements of deflection force for optical-fibre-embedded arrays with and without wires gave an increase in deflection force that was comparable to the effect of the embedding.

The results in Fig. 7c show the effect of embedding on the deflection force for the 50 µm diameter optical fibre. As can be seen from the results, embedding a 50 µm optical fibre into an electrode array increases the deflection force of the optical fibre compared to plain fibre alone. This supports the theory that embedding a 50 µm optical fibre into an electrode array will have little effect on the overall stiffness of the array as the Silastic component of the array itself contributes the majority of the stiffness. The increase due to embedding in Fig. 7c is more significant than the corresponding increase in Fig. 7b. In general the derived theory supports the measured differences. However, the level of agreement seen drops off for smaller values of load location on the plain fibre and for larger values of load location on the embedded fibre.

4.2 Buckling Force

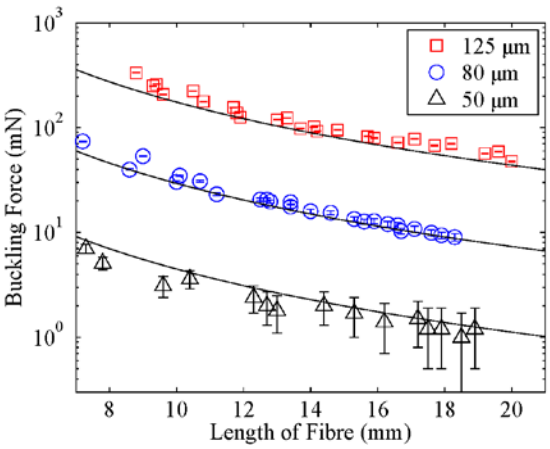

Fig. 8. Results of the buckling testing of the optical fibres, together with curves calculated from the theory. Note that smaller lengths could not be measured as the forces for the 125 µm fibre were above the range of the force sensor.

Measurements of buckling force for optical fibres with 90° cleaved tips are shown in Fig. 8, for fibre lengths between 9 mm and 20 mm (125 µm fibre) and 7 mm and 18 mm (80 µm and 50 µm fibre). As expected the force required to buckle the fibre was found to decrease as the fibre diameter decreased. Also shown in Fig. 8 are theoretical curves (Eq. 3). Good agreement was obtained between the recorded data and the theory for the 125 µm, 80 µm and 50 µm optical fibres, with R^2 values of 0.799, 0.928 and 0.717 respectively.

4. Discussion

Measurements of deflection force were performed on human, animal and custom cochlear electrode arrays containing optical fibres. The aim of the work was to evaluate the forces required to bend the arrays, as bending is required during insertion in the cochlea. Deflection and buckling tests provide a measure of loads applied in the transverse and longitudinal directions respectively. During electrode array insertion the interaction and resulting forces between the array and the delicate cochlear structure are critical to determining whether trauma will ensue. As electrode arrays containing embedded optical fibre(s) may offer additional functionality, it is important to understand the resulting mechanical properties in order to help evaluate their potential to cause harm.

The deflection forces of the electrode arrays with embedded optical fibres followed the expected trend, with greater force required to bend the array as the diameter of the embedded optical fibre increased. The results suggest that the stiffness properties of the optical-fibre-embedded electrode arrays were dominated by the properties of the optical fibre. However the measured results are affected by a number of factors, including the position of the embedded components, the presence of wires and friction with the force sensor. For the custom optical fibre electrode arrays tested, the effect of Silastic embedding on the optical fibre deflection force reduced as the diameter of the fibre increased. The addition of wires and the Silastic embedding material appeared to have a similar effect on the resulting deflection forces. The recorded data showed reasonable agreement with

both the cantilever beam theory and the derived theory. In general the derived theory provided better agreement with the recorded results, but is still not perfect. More detailed modelling is required to better improve the fit. Such modelling is outside the scope of the paper.

Despite playing a key role in cochlear electrode research and development, the mechanical properties of animal electrode arrays have not been reported previously. The deflection force data for the various electrode arrays tested (human, animal and custom) highlighted some key differences in response. For each of the animal array types tested, the forces required to deflect the arrays were lower than the human straight array tested. This is most likely due to the smaller number of wires contained in the animal electrode arrays.

When comparing the deflection forces for the different electrode array types, the custom optical fibre electrode arrays containing 125 μm and 50 μm diameter fibre bracketed the measurements for the human and animal electrode arrays and the 80 μm diameter fibre custom array was in the middle of the range. This suggests that optical fibre diameters of 50 μm or less can be used in a cochlear implant without affecting the stiffness properties of the array. With additional testing it may be possible to identify other fibre diameters between 50 μm and 80 μm that have a negligible effect on the arrays stiffness.

Unlike the optical-fibre-embedded electrode arrays, the deflection force results for animal and human wired electrode arrays without embedded optical fibre do not follow the curve shape of the cantilever theory. This is believed to arise from the non-uniform stiffness of the electrode arrays due to the changing number of wires along the array length and other mechanical design properties aimed at the minimisation of insertion trauma [33]. While it may be possible to model the non-uniform structure more accurately, for example by using the rule of mixtures [44] or finite element analysis [4], the distinction is not critical for the main conclusions presented here. Given that the overall stiffness of the electrode array appears to be dominated by the stiffest component, further work may be required to understand how the introduction of an optical fibre with uniform stiffness affects the properties of more complex array structures.

The results of buckling force tests on optical fibres followed a similar trend to the deflection force tests in which the force required to bend the optical fibre decreased as the diameter of the embedded optical fibre got smaller. Indeed the experimental data was found to agree well with the results predicted from theory. Difficulties were encountered when attempting to measure the buckling force of the human and animal electrode arrays as their low stiffness and natural tendency to curve made the testing procedure invalid. This may also explain why there is a lack of published work looking at the buckling force of cochlear electrode arrays.

It is useful to briefly discuss the results obtained in the context of the level of force applied during insertion that might lead to trauma. This is a complicated issue as a combination of different forces can act during insertion, including transverse, longitudinal and frictional forces. Mechanical measurements of rupture force on the human basilar membrane were found to be 26-35 mN [45], while forces greater than ~50 mN measured at the tip of a custom guinea pig electrode tended to result in trauma [9]. In another study [8], insertion tests on human temporal bones showed trauma when multiple 55 μm diameter optical fibres were inserted at the same time (corresponding to measured insertion forces $\geq$ 50 mN). Using Figs. 5 and 8 it is relatively easy to match the combinations of optical fibre diameter and corresponding effective length of fibre for which forces lower than say ~50 mN cause bending to occur, which may result in trauma being avoided.

In this work the human array used for comparison was a common straight array design. It is worth noting that there are a range of other cochlear array designs (e.g. Contour Advance Electrode, Cochlear Ltd [43]) which have different stiffness properties [33]. Therefore caution must be exercised when attempting to draw general conclusions about the results obtained here and cochlear electrode arrays in general.

Finally it is worth mentioning that the measurements obtained for the deflection and buckling forces of optical fibres have broader implications than just the application to cochlear implants. There are, for example, a wide range of optical fibre sensors which are potentially subject to transverse and compressive forces which, if they cause the fibre to buckle, may affect the sensor measurement [46]. The data provided in this work provides

indications of the maximum force that can be exerted on an optical fibre sensor for a given length and fibre diameter before potentially detrimental bending occurs.

5. Conclusion

The results obtained in this work suggest that an optical fibre with a diameter of approximately 50 µm or less embedded into a fully wired cochlear electrode array should not greatly affect the stiffness profile of the electrode array. This suggests that the incorporation of optical fibre into cochlear electrode arrays, for use in sensing or optical stimulation applications for example, should be feasible. However, further studies using optical-fibre-embedded arrays are required to determine if there are any differences in insertion trauma compared to standard electrode arrays.

Acknowledgements

The authors would like to thank Helen Feng at the Bionics Institute for manufacturing the embedded electrode arrays and use of equipment; Mark Kivinen, Yeannette Lizama and Kristian Fenech from Swinburne for their technical assistance and Cochlear Ltd for providing the Nucleus straight array. The Bionics Institute acknowledges the support it receives from the Victorian Government through its Operational Infrastructure Support Program. This work was supported in part by the Australian Research Council through Linkage Project LP120100264 and Industrial Transformation Training Centre IC140100023.

References

[1] Clark GM. Cochlear implants: Fundamentals and applications. New York: Springer Verlag 2003.
[2] Clark GM. Personal reflections on the multichannel cochlear implant and a view of the future. J Rehabil Res Dev. 2008;45:651-94.
[3] Kha H, Chen, B. Finite element analysis of damage by cochlear implant electrode array's proximal section to the basilar membrane. Otol Neurotol. 2012;33:1176-80.
[4] Chen BK, Clark, G.M., Jones, R. Evaluation of trajectories and contact pressures for the straight nucleus cochlear implant electrode array - A two-dimensional application of finite element analysis. Med Eng Phys. 2003;25:141-7.
[5] Kha HN, Chen, B.K., Clark, G.M. 3D finite element analyses of insertion of the Nucleus standard straight and the Contour electrode arrays into the human cochlea. J Biomech. 2007;40:2796-805.
[6] Lim YS, Park, S. I., Kim, Y. H., Oh, S. H., Kim, S. J. Three-dimensional analysis of electrode behavior in a human cochlear model. Med Eng Phys. 2005;27:695-703.
[7] Patrick JF, MacFarlane, J. C. Characterization of mechanical properties of single electrodes and multielectrodes. Clark and Bushby, editors, International Cochlear Implant Symposium. 1987:46-8.
[8] Shepherd RK, Clark, G. M., Pyman, B. C., Webb, R. L. Banded intracochlear electrode array: Evaluation of insertion trauma in human temporal bones. Ann Oto Rhinol Laryn. 1985;94:55-9.
[9] Wade SA, Fallon JB, Wise AD, Shepherd RK, James N, Stoddart PR. Measurement of forces at the tip of a cochlear implant during insertion. IEEE T Bio-Med Eng. 2014.
[10] Tykocinski M, Cohen LT, Pyman BC, Roland Jr T, Treaba C, Palamara J, et al. Comparison of electrode position in the human cochlea using various perimodiolar electrode arrays. American Journal of Otology. 2000;21:205-11.
[11] Rebscher SJ, Hetherington, A., Bonham, B., Wardrop, P., Whinney, D., Leake, P. A. Considerations for design of future cochlear implant electrode arrays: Electrode array stiffness, size, and depth of insertion. J Rehabil Res Dev. 2008;45:731-48.
[12] Wardrop P, Whinney, D., Rebscher, S. J., Roland Jr, J. T., Luxford, W., Leake, P. A. A temporal bone study of insertion trauma and intracochlear position of cochlear implant electrodes. I: Comparison of Nucleus banded and Nucleus Contour™ electrodes. Hear Res. 2005;203:54-67.
[13] Podskarbi-Fayette R, Pilka A, Skarzynski H. Electric stimulation complements functional residual hearing in partial deafness. Acta Oto-Laryngol. 2010;130:888-96.
[14] Skarzynski H, Lorens A, Piotrowska A, Anderson I. Preservation of low frequency hearing in partial deafness cochlear implantation (PDCI) using the round window surgical approach. Acta Oto-Laryngol. 2007;127:41-8.
[15] Gstoettner W, Kiefer J, Baumgartner WD, Pok S, Peters S, Adunka O. Hearing preservation in cochlear implantation for electric acoustic stimulation. Acta Oto-Laryngol. 2004;124:348-52.

[16] Skarzynski H, Podskarbi-Fayette R. A new cochlear implant electrode design for preservation of residual hearing: A temporal bone study. Acta Oto-Laryngol. 2010;130:435-42.
[17] James C, Albegger K, Battmer R, Burdo S, Deggouj N, Deguine O, et al. Preservation of residual hearing with cochlear implantation: How and why. Acta Oto-Laryngol. 2005;125:481-91.
[18] Turner CW, Reiss LA, Gantz BJ. Combined acoustic and electric hearing: Preserving residual acoustic hearing. Hear Res. 2008;242:164-71.
[19] Roland JT. A model for cochlear implant electrode insertion and force evaluation: Results with a new electrode design and insertion technique. The Laryngoscope. 2005;115:1325-39.
[20] Zhang J, Wei, W., Ding, J., Roland, T., Manolidis, S., Simaan, N. Inroads toward robot-assisted cochlear implant surgery using steerable electrode arrays. Otol Neurotol. 2010;31:1199-206.
[21] Schurzig D, Labadie, R. F., Hussong, A., Rau, T. S., Webster III, R. J. Design of a tool integrating force sensing with automated insertion in cochlear implantation. IEEE/ASME Transactions on Mechatronics. 2012;17:381-9.
[22] Li E, Yao, J. Fiber-optic bending sensor for cochlear implantation. Fourth International Conference on Photonics and Imaging in Biology and Medicine. Tianjin, China 2006.
[23] Wu Y. Sensors and actuators for the cochlear implant using inherently conducting polymers [PhD]: University of Wollongong; 2006.
[24] Tang Y, Aslam, D. M., Wang, J., Wise, K. D. New design of the cochlear implant probe with polycrystalline diamond piezoresistive position sensors. 1st IEEE International Conference on Nano/Micro Engineered and Molecular Systems. Zhuhal, China 2006. p. 1129-32.
[25] Wang J, Wise, K. D. A thin-film cochlear electrode array with integrated position sensing. J Microelectomech S. 2009;18:385-95.
[26] Wise KD, Bhatti, P. T., Wang, J., Friedrich, C. R. High-density cochlear implants with position sensing and control. Hear Res. 2008;242:22-30.
[27] Zhang A, Clark, G. M., Pyman, B. C., Brown, M., Zmood,R The development of a tympanic membrane sensor for a totally implantable cochlear implant or hearing aid. In Cochlear Implants: XVI World Congress of Otohinolaryngology Head and Neck Surgery. Sydney, Australia: Monduzzi Editore; 1997. p. 109-12.
[28] López H. Handbook of Optical Fibre Sensing Technology: Chichester : Wiley 2002.
[29] Richter CP, Matic, A. I., Wells, J. D., Jansen, E. D., Walsh, J. T. Neural stimulation with optical radiation. Laser Photonics Rev. 2011;5:68-80.
[30] Thompson AC, Wade, S. A., Pawsey, N. C., Stoddart, P. R. Infrared neural stimulation: Influence of stimulation site spacing and repetition rates on heating. IEEE T Bio-Med Eng. 2013;60:3534-41.
[31] Thompson AC, Wade, S. A., Brown, W. G., Stoddart, P. R. Modeling of light absorption in tissue during infrared neural stimulation. J Biomed Opt. 2012;17:075002.
[32] Balster S, Wenzel GI, Warnecke A, Steffens M, Rettenmaier A, Zhang K, et al. Optical cochlear implant: evaluation of insertion forces of optical fibres in a cochlear model and of traumata in human temporal bones. Biomedizinische Technik Biomedical engineering. 2014;59:19-28.
[33] Kha HN, Chen, B. K., Clark, G. M., Jones, R. Stiffness properties for Nucleus standard straight and contour electrode arrays. Med Eng Phys. 2004;26:677-85.
[34] Baumgart F. Stiffness — an unknown world of mechanical science? Injury. 2000;31, Supplement 2:14-84.
[35] Oberg E, Jones, F. D., Horton, H. L., Ryffell, H. H. Machinery's Handbook (26th Edition): Industrial Press; 2000.
[36] Mohammad N, Szyszkowski, W., Zhang, W. J., Haddad, E. I., Zou, J., Jamroz, W., Kruzelecky, R. Analysis and development of a tunable fiber Bragg grating filter based on axial tension/compression. J Lightwave Technol. 2004;22:2001-13.
[37] Mott R. Applied strength of materials. Upper Saddle River, New Jersey: Pearson Education; 2008.
[38] Lu W, Xu, J., Shepherd, R. K. Cochlear implantation in rats: A new surgical approach. Hear Res. 2005;205:115-22.
[39] Shepherd RK, Xu, J. A multichannel scala tympani electrode array incorporating a drug delivery system for chronic intracochlear infusion. Hear Res. 2002;172:92-8.
[40] Shepherd RK, Coco, A., Epp, S. B. Neurotrophins and electrical stimulation for protection and repair of spiral ganglion neurons following sensorineural hearing loss. Hear Res. 2008;242:100-9.
[41] Xu J, Shepherd, R. K., Millard, R. E., Clark, G. M. Chronic electrical stimulation of the auditory nerve at high stimulus rates: A physiological and histopathological study. Hear Res. 1997;105:1-29.
[42] Shepherd RK, Verhoeven, K., Xu, J., Risi, F., Fallon, J., Wise, A. An improved cochlear implant electrode array for use in experimental studies. Hear Res. 2011;277:20-7.
[43] Cochlear. Cochlear™ Nucleus® Electrode Portfolio, Reference Guide. http://www.cochlear.com/wps/wcm/connect/81f19b2d-8a73-42fb-9c12-1d214de5d2c8/ElectrodePortfolioSellSheet.pdf?MOD=AJPERES&CACHEID=81f19b2d-8a73-42fb-9c12-1d214de5d2c82012.

[44] Askeland DR. The Science and Engineering of Materials. 6th ed. ed: Stamford, CT : Cengage Learning; 2011.
[45] Ishii T, Takayama M, Takahashi Y. Mechanical properties of human round window, basilar and Reissner's membranes. Acta Oto-Laryngol, Supp. 1995:78-82.
[46] Thompson AC, Cadusch PJ, Robertson DF, Stoddart PR, Wade SA. Origins of spectral changes in fiber Bragg gratings due to macrobending. J Lightwave Technol. 2012;30:3500-11.